ACS APPLIED MATERIALS & INTERFACES

Research Article

Cite This: ACS Appl. Mater. Interfaces XXXX, XXX, XXX−XXX

www.acsami.org

Electrostatic Transparent Air Filter Membranes Composed of Metallized Microfibers for Particulate Removal

Min-Woo Kim,[†,§] Seongpil An,[‡,§] Hyunjun Seok,[†] Sam S. Yoon,[*,†] and Alexander L. Yarin[*,‡]

[†]School of Mechanical Engineering, Korea University, Seoul 02841, Republic of Korea

[‡]Department of Mechanical and Industrial Engineering, University of Illinois at Chicago, 842 W. Taylor Street, Chicago, Illinois 60607-7022, United States

Supporting Information

ABSTRACT: Particulate matter (PM) from ever-increasing industrialization poses a great public health risk. Although fiber-based filters are used effectively to block PM, filters with high packing densities suffer from excessive pressure drops. Electret filters bypass intermediate- or large-sized particles and thus capture only small particles, the motion of which can be influenced by weak electrostatic fields. In this study, we demonstrate the fabrication of metallized fibers that produce intense electric fields, thereby enabling capture of PMs of a variety of sizes produced by burning incense. The filter consisting of these metallized fibers effectively removes moving particles from air. An electricity-driven filter is relatively thin and has a low packing density, making it light, portable, transparent, and inexpensive. The sizes of the pores between the metallized fibers are readily controlled by manipulating the electrospinning and electroplating times. Sufficiently large pores permit efficient airflow and thus increase permeability without risking an excessive pressure drop. The metallized fiber filter is washable and thus reusable. In this study, a PM removal rate of >97% was recorded using a filter designed under optimal conditions.

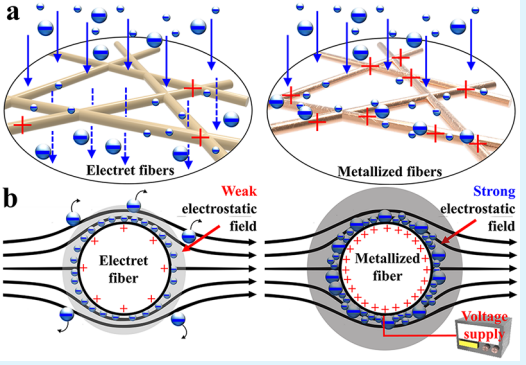

KEYWORDS: *metallized microfibers, air filtration, electrostatic attraction, particulate matter, reusable filter*

1. INTRODUCTION

Global industrialization and population growth have given rise to airborne pollutants and particulate matter (PM) that pose serious health risks, especially to elders and children whose respiratory functions are vulnerable to pollution.[1−7] Heating and power generation systems produce nitrogen dioxide and sulfur dioxide. Gas cooking, cigarette smoke, and commuting by car all produce carbon monoxide. Volatile organic compound emissions are produced from indoor materials such as paint, furniture, and petrochemical products.[8] $PM_{2.5}$ refers to particles that are <2.5 μm in size, which are particularly harmful because of their efficiency in penetrating human bronchi, lungs, trachea, bronchioles, and alveoli.[9,10] In addition, microorganisms such as bacteria, viruses, and fungi can become easily attached to $PM_{2.5}$, which function as carcinogens. These complicate countertreatments.[10−14]

Today, fibrous filters account for >70% of the air filter market.[15] Fiber filters can capture submicrometer particles through multiple layers of fibers. The physical properties of these fibers, such as the diameter, packing density, thickness, and alignment, are critical in determining the filter efficiency.[16] In particular, reducing the fiber size favorably affects filtration because it decreases the basis weight and pore size while increasing the specific surface area and pore interconnectivity, thereby increasing the contact probability. For these reasons, nanoscale fibers fabricated by electrospinning, solution blowing, and supersonic solution blowing have received considerable attention from air filter industries[17−24] and research community.[25−27]

Filters using high-packing-density nanoscale fibers can experience low air permeability, increased air resistance, high pressure drops, and high operating pressures that result in high energy consumption, filter clogging, and reduced filter service lifetimes.[19] Therefore, designing filters with low packing densities and high permeability that retain the ability to capture submicrometer particles is imperative. This goal can be achieved by electrical charging of filters, which induces the electrically driven motion of particles of different sizes, as described in Figure 1. Many particles carry an electric charge. Moreover, natural or accidental radioactivity can induce charge accumulation on radioactive particles.[28]

Polymer electret filters capture particles by both nonelectrical filtration mechanisms and electrostatic attraction, as shown in Figure 1a,b. Physical filtration occurs by impaction, interception, and diffusion, whereas electrical filtration utilizes an electric field imposed by charged airborne particles and/or the filter itself. These polymeric dielectric materials include polyethylene,

Received: April 1, 2019
Accepted: July 1, 2019
Published: July 1, 2019

DOI: 10.1021/acsami.9b05686
ACS Appl. Mater. Interfaces XXXX, XXX, XXX−XXX

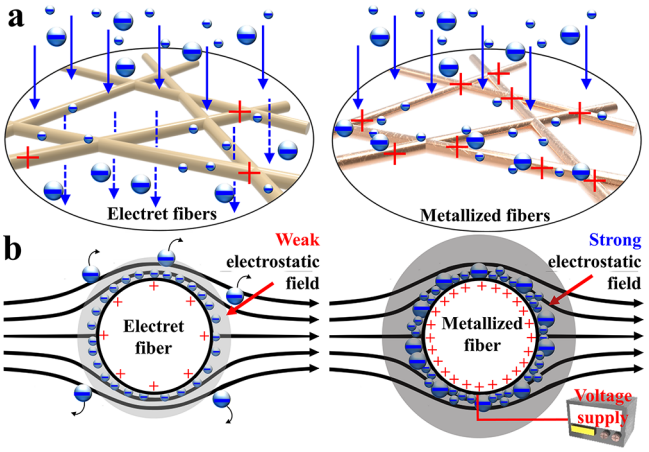

Figure 1. (a) Comparison of air filtration performance by electret vs metallized fibers. (b) Air filtration using a weak electrostatic field from electret fibers vs a strong electrostatic field associated with metallized fibers.

polypropylene, and poly(tetrafluoroethylene) and have quasi-permanent electrical charges that facilitate particle attraction.[29]

Electret is a material that generates a permanent electric field without an externally applied voltage. Electret filters produce a strong electrostatic field close to the surface of the fiber, enabling fine particles to be removed with higher efficiency than when employing conventional mechanical filtering.[30−33] The advantage of electret filters is that they can achieve better trapping as compared to mechanical filtering because of electrostatic attraction. Electret filters usually have a low density, and therefore, the pressure drop of 1−200 Pa for an air face velocity of 0.05 m/s is typical. By contrast, the disadvantage of the electret filter is that the attraction is reduced when the fibers are covered with particles.[30,34] Recently, various studies have been performed on filters that utilize electrical charges. The filters can purify polluted air environments by the mechanism shown in Figure 1a.

However, electret filtration with polymer nanofibers has some drawbacks, namely, low-level charge and rapid charge decay due to the low weight of the fibers.[21] Enhancing the dielectric properties of fibers has been attempted by modifying their physical structures and adding inorganic electrets to them.[20,21,35−38] These studies have also investigated the effects of polymer dielectric properties on the filtration performance. Although these attempts to improve the electrical properties of fibers have gradually advanced the filtration technology, the intrinsic shortcomings of electret filters remain as challenges to overcome.

Figure 1a,b compares the particle filtration mechanisms based on dielectric fibers to those for metallized fibers. The comparison shows that metallized nanofibers can in principle be more effective at particle removal than electret filters consisting of dielectric materials simply because metallized fibers can provide stronger electric fields that attract more particles.

For these reasons, we propose the use of metallized microfibers[39−41] to provide sufficiently strong electric fields between charged particles and filter fibers. We demonstrate that particles of all sizes are practically instantaneously attracted to metallized fibers under applied electric fields. Carbon monoxide or/and dioxide gaseous products from burning incense are used as sample particles captured by the metallized fibers under the applied electric field. The metallized fiber filter has a very low packing density and thus allows high permeability, a low pressure drop, and no clogging until all pores are filled with filtered particles. Because the filter is relatively thin with a low packing density, it is readily washable and reusable. Metallized fibers of several micrometers in diameter are used in a filter, generating very strong electric repulsion and attraction depending on the polarity. Parametric studies reported herein include the metallized fiber fabrication process, optimization of packing density, and optimization of fiber location inside a cylindrical filter. It should be emphasized that no particle precharging was conducted in this study, and particle reaction to the electric field associated with the proposed metallized filter showed that the particles were originally charged.

2. EXPERIMENTAL METHODS

2.1. Cu Microfibers. Cu-plated microfibers were fabricated by employing the subsequent processes of electrospinning and electroplating, as previously studied by the present group.[39,40,42−47] The electrospinning solution was prepared by dissolving 8 wt % of polyacrylonitrile [PAN, $(C_3H_3N)_n$; M_w = 150 kDa; Sigma-Aldrich] pellets in *N*,*N*-dimethylformamide (DMF, 99.8%; Sigma-Aldrich) and then stirring the mixed solution for 24 h at room temperature of 24 °C. The 8 wt % PAN solution was electrospun with a fixed flow rate (Legato 100, KDS) and a fixed applied DC voltage (EL20P2, Glassman High Voltage Inc.). Details of the electrospinning conditions are listed in Table 1.

Table 1. Operating Conditions for the Electrospinning and Electroplating

process	parameters	values
electrospinning	applied DC voltage (kV)	6
	flow rate (μL/h)	280
	nozzle-to-collector distance (cm)	13
	electrospinning time (s)	60
electroplating	applied voltage (kV)	3
	nanofiber mat-to-Cu electrode distance (cm)	3
	electroplating time (s)	0, 10, 30, 60

For the Cu electroplating of the electrospun PAN nanofibers, a Cu electroplating solution was first prepared by mixing 80 g of copper sulfate (Sigma-Aldrich), 25 g of sulfuric acid (Matsunoen Chemicals), 2.5 g of hydrochloric acid (Sigma-Aldrich), 50 g of formaldehyde (Sigma-Aldrich), and 500 mL of distilled water. The solution was stirred for 1 h at room temperature to make it homogeneous.

Before PAN nanofibers were electroplated, they were metal-seeded by sputtering with Pt at a thickness of a few nanometers, which induced minimal conductivity in the polymer electrospun nanofibers. A DC power supply (E3664A, Agilent Technologies) and homemade electroplating setup were used for the Cu electroplating. Details of the electroplating conditions are listed in Table 1. The as-Cu-plated nanofibers were rinsed with distilled water and dried by a N_2 gas gun.

2.2. Characterization. The morphology and elemental mapping of Cu microfibers were explored by high-resolution scanning electron microscopy and energy-dispersive X-ray spectroscopy (XL30 SFEG, Phillips Co., Holland) at 15 kV. The transmittance (T) of the Cu microfiber was measured using a UV−vis spectrophotometer (Optizen POP, Mecasys, Daejeon, Korea). The transmittance was measured in the wavelength range of 350−1100 nm, which includes the visible light region. Note that the basic condition (T = 100%) was based on two slide glasses. The transmittance of the Cu microfiber filter was measured by inserting the Cu microfiber filter between two slide glasses. The fiber diameters and porosities of the Cu microfibers were measured from SEM images using the I-Measure 3 software. The carbon monoxide (CO) concentration of the generated smoke was measured

DOI: 10.1021/acsami.9b05686
ACS Appl. Mater. Interfaces XXXX, XXX, XXX−XXX

by a gas detector (QRAE 3 of RAE systems). Two PMs from an incense stick and charcoal were used for the filtration tests in this study: one was from the smoke of a burning incense stick and the other was prepared by crushing charcoal and sieving it. Specifically, a mortar was used to crush a bulk charcoal to obtain small charcoal powders with diameters of less than 500 μm. Then, the crushed charcoal powders were sifted using a 50 μm sieve.

2.3. Smoke Filtration Test. To demonstrate the filtering performance of the Cu microfibers, a cylindrical setup was built, as shown in Figure 2a. A Cu microfiber filter and 30 s electrospun PAN

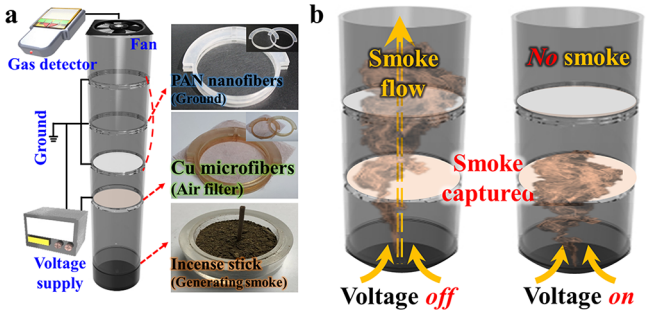

Figure 2. (a) Schematic and photographs of the smoke filtration setup. (b) Operating principle of the smoke filtration setup.

nanofiber mat were installed inside the cylindrical setup and fixed by an acryl supporting agent. The Cu microfiber filter here was employed as a powered electrode that could capture the charged PM, and the 30 s electrospun PAN nanofiber mat was used as a grounded electrode. An incense stick was placed at the bottom of the setup to induce buoyancy-driven smoke flow from the bottom to the top of the setup.

Figure 2b shows the operating principle of the proposed electrostatic filter without and with applied voltage. At the top of the cylindrical setup, a fan and gas detector were installed to induce laminar flow in the cylinder and to measure the CO concentration in the passing smoke. The air flow rate was determined by the power input to the fan. Thus, the air flow rate was fixed and stabilized both the incense burning process and oxygen concentration at the bottom inlet. In addition, the amount of CO gas produced from the burning incense was proportional to the amount of PM produced from the same incense burning.[48] It should be emphasized that the measured concentration of CO was not used here as a measure of the amount of PM resulting from incense burning. To characterize the filtration of PM, a separate experiment with charcoal particles was performed, which is described as follows.

It should also be emphasized that in free carbon monoxide, a net negative charge remains at the carbon end, and the molecule possesses a small dipole moment.[49] In our study, this caused deposition of CO molecules from the incense smoke on the Cu microfiber filter when positive voltage was applied. Deposition of water vapor was also caused by the polarization of water molecules. In addition, burning resulted in the formation of multiple charged radicals.[50] Their coagulation in the Cu microfiber filter in turn generates PMs.

3. RESULTS AND DISCUSSION

3.1. Cu Microfiber Filter. Figure 3a shows a schematic of electrospinning and electroplating for Cu microfiber fabrication. The microfibers were fabricated by electrospinning followed by fiber electroplating (cf. Experimental Methods Section). Previous studies by the present group demonstrated that Cu microfibers fabricated by this combined approach consisted of pure Cu and possessed diameters dependent on the fiber diameter of electroplating times.[40,42−45] The comparison of the fiber diameters versus electroplating times is shown in Figure 3b. The average fiber diameter was determined in each case by measuring 100 microfibers in the SEM images. The average diameters were 0.53 ± 0.027, 2.24 ± 0.096, 3.83 ± 0.178, and

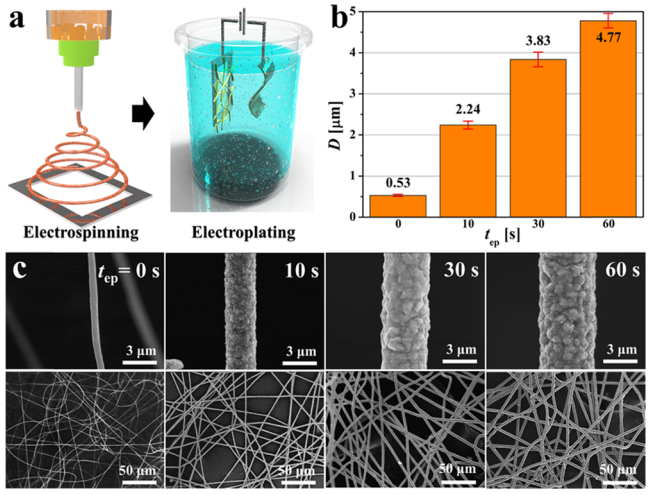

Figure 3. (a) Schematic of the Cu microfiber fabrication process (electrospinning and electroplating). (b) Diameters of Cu microfibers vs Cu electroplating times. (c) SEM images.

4.77 ± 0.178 μm at 0, 10, 30, and 60 s electroplating times, respectively. The first row of SEM images in Figure 3c shows the Cu microfibers obtained with different electroplating times (t_{ep}). The average diameter of the nonplated PAN nanofibers (at t_{ep} = 0 s) was 500 ± 0.027 nm. Figure 3c shows that the fiber diameter increased with increasing Cu plating times at t_{ep} = 10, 30, and 60 s.

3.2. Electrostatic Smoke Filtration by Cu Microfiber Filter. The Cu microfiber filter was located under the bottom position (B), and the PAN nanofiber mat could be installed at one of the three locations of either top (T), middle (M), or near the bottom (B) of the setup, as shown in Figure 4. Figure 4

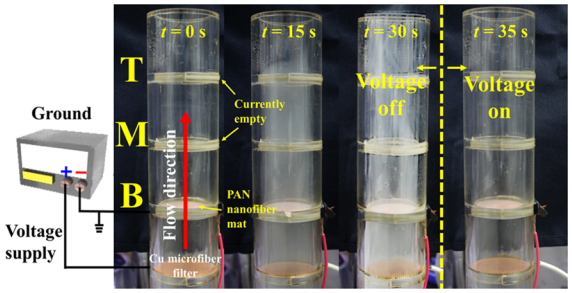

Figure 4. Smoke filtration before and after applying voltage of 20 kV. T, M, and B denote the top, middle, and bottom positions, respectively, of the PAN nanofiber mat in the cylindrical setup. Here, the PAN nanofiber mat is installed at the bottom position.

shows that smoke generated by burning incense rose through the setup. At this time, smoke particles passing through the Cu microfiber filter were negatively charged by the electrostatic induction effect (cf. Section 2.3).[51−53] The negatively charged smoke particles were accumulated at the positively charged Cu microfiber filter as the voltage supply was turned on.

The smoke filter performance was confirmed by measuring the CO concentration every 30 s based on the assumption that the particle concentration was proportional to that of CO. Figure 4 shows the time-dependent flow of smoke in the presence or absence of voltage. For the uncharged Cu microfiber filter, smoke penetrated both the Cu microfiber filter and PAN nanofiber mat en route to the setup exit. By contrast, the high

DOI: 10.1021/acsami.9b05686
ACS Appl. Mater. Interfaces XXXX, XXX, XXX−XXX

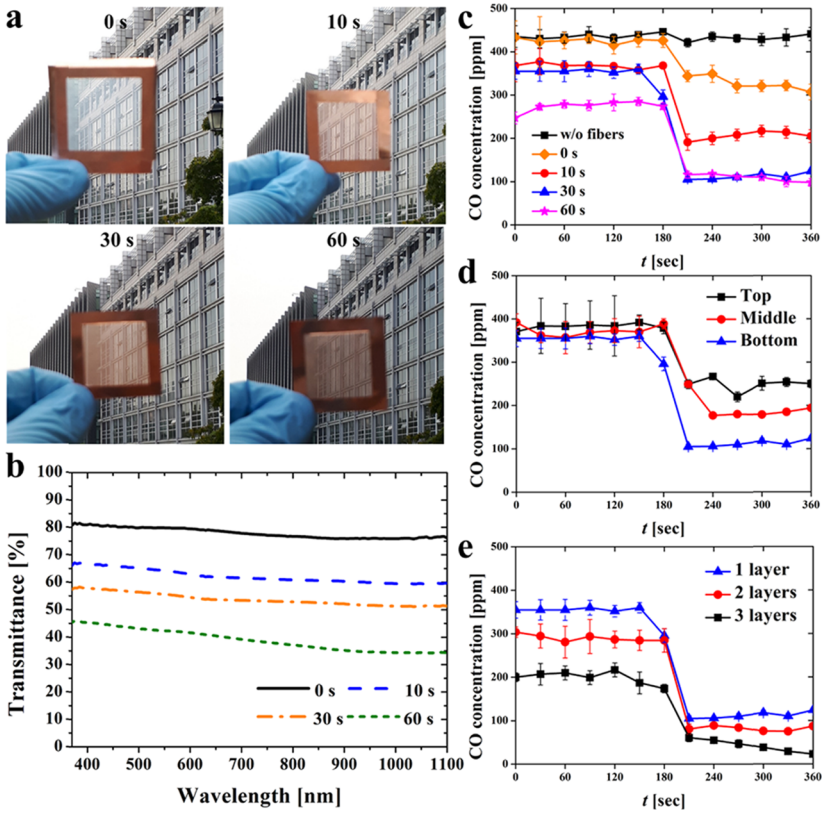

Figure 5. (a) Photographs and (b) transmittance spectra of the Cu microfiber filter formed with different electroplating times of t_{ep} = 0, 10, 30, and 60 s. Changes in CO concentration as a function of (c) t_{ep}, (d) position of the PAN nanofiber mat in the setup (cf. Figure 4b), and (e) number of Cu microfiber filters installed in the setup. In the cases of (d) and (e), the electroplating time is t_{ep} = 30 s.

voltage applied between the Cu microfiber filter and PAN nanofiber mat facilitated the capture of charged PMs by the filter (see the fourth photograph in Figure 4 and the Supplementary Video 1).

Figure 5a shows photographs of Cu microfiber filters formed with different electroplating times, demonstrating that all Cu microfiber filters had high transparencies. This implies that the filters were very thin and could not cause a significant additional pressure drop, which is beneficial for applications requiring high permeability and lightness (where the pressure drop on a filter decreases with its thickness). Note also that the electrical conductivity of these metallized nanofibers was not lost up to strains of 600%.[43] Figure 5b shows the light transmittance (T) versus wavelength of Cu microfibers formed with different electroplating times. When t = 0 (no metallization), T at 550 nm (in the visible range) was approximately 80%. As the electroplating time increased to t_{ep} = 10, 30, and 60 s, T decreased to 64, 56, and 42%, respectively.

Figure 5c–e shows the smoke filtration performance of different setups with Cu microfibes. The mean results from five repeated experiments in each case were compared. The changes in CO concentration were measured for 360 s; in every case, the voltage of 20 kV was applied only during the last 180 s. In Figure 5c, the CO concentration without the Cu microfiber filter (see the without-fiber case in Figure 5c) yielded constant values of 425–440 ppm for 360 s, whereas the CO concentration did not decrease even after the voltage was applied as no Cu microfiber filter and no electric field were accordingly formed in the setup. When t_{ep} = 0 s, as shown in Figure 5c which corresponds to the bare PAN nanofiber mat, a similar CO concentration was observed in comparison with the without-fiber case before the voltage was applied, whereas the concentration slightly decreased to 307–349 ppm after a voltage of 20 kV was applied. This suggests that the charged bare fibers operated as electret materials. For the Cu microfiber filter electroplated for t_{ep} = 10 s, a slightly lower CO concentration compared to that of the previous cases was exhibited before the voltage was applied, where the corresponding concentration was in the range of 358–377 ppm. In contrast to the previous cases, as the voltage of 20 kV was applied to the Cu microfiber filter, the corresponding CO concentration significantly decreased to 191–217 ppm.

A dramatic drop in CO concentration after the voltage was applied was also observed in both cases of t_{ep} = 30 and 60 s, where nearly identical CO concentrations in the range of 105–124 ppm were measured (see the 30 and 60 s cases in Figure 5c) after a voltage of 20 kV was applied. However, it should be emphasized that a noticeable difference in CO concentration between the t_{ep} = 30 and 60 s samples was observed before the voltage was applied. At t = 0, the CO concentration with the t_{ep} = 30 s sample was reduced by 234 ppm from the time before to the time after the voltage was applied, whereas that of the t_{ep} = 60 s sample was reduced by 169 ppm (cf. Table 2).

Because the porosity of specimens varies with the electroplating time, different filtration performances associated with CO concentration before the voltage was applied were observed in different cases. To characterize the porosity values of the specimens, we analyzed SEM images of each case (cf. Experimental Methods Section). A porosity value was obtained by dividing the area without fibers in the SEM image by the total area of the corresponding SEM image. The calculated porosity values of the 0, 10, 30, and 60 s cases shown in Figure 5c were 82.2, 71.5, 63.9, and 48.9%, respectively.

DOI: 10.1021/acsami.9b05686
ACS Appl. Mater. Interfaces XXXX, XXX, XXX–XXX

Table 2. Filtration Efficiency

condition	case	CO concentration (ppm) before	CO concentration (ppm) after	efficiency (%)
(a) plating time	without nanofibers	430	430	
	0 s (PAN fibers without plating)	425	327	22.9
	10 s	368	206	44.0
	30 s	346	112	67.6
	60 s	278	109	60.8
(b) location (single layer)	B	346	112	67.6
	M	342	218	36.3
	T	385	249	35.4
(c) *N* of Cu microfiber layers	1	346	112	67.6
	2	287	82	71.5
	3	199	42	78.8

To better characterize the performances of the Cu microfiber filters, the results of additional experiments (at t_{ep} = 30 s) are shown in Figure 5d–e. Figure 5d shows the results of CO concentration with different locations of the grounded PAN nanofiber mat in the pipe near the bottom (B), in the middle (M), and at the top (T) of the setup (see Figure 4b). When the PAN nanofiber mat was installed at T, the average CO concentration before the voltage was applied was 385 ppm. As the PAN nanofiber mat was lowered to B, the CO concentration before the voltage was applied slightly decreased to 362 and 346 ppm for the M (red circles) and B (blue triangles) locations, respectively. The CO concentrations after the voltage of 20 kV was applied were 249, 218, and 112 ppm at the T, M, and B locations, respectively. In other words, the filtering performance diminished as the distance between the Cu microfiber filter and grounded PAN nanofiber mat increased due to the reduced strength of the electric field.

Figure 5e shows the CO concentration profiles with different numbers of Cu microfiber filters, where N_{layer} = 1, 2, and 3. In each case, the PAN nanofiber mat was placed at the B-marked position of the setup shown in Figure 4b, and different numbers of superimposed Cu microfiber filters were placed below the B-marked position (cf. Figure 4b). For two Cu microfiber filters, the CO concentrations of 287 ppm (before the voltage was applied) and 82 ppm (after the voltage was applied) were recorded. For the three filters, 199 ppm (before the voltage was applied) and 42 ppm (after the voltage was applied) were recorded. Before the voltage was applied, the CO concentration was reduced by increasing the number of Cu microfiber filters as the permeability decreased when increasing the number of layers.

The filtration efficiency η was defined using the ratio of the CO concentration C with applied voltage to that without applied voltage. C_0 and C denote the average values in CO concentration before and after the voltage was applied. Thus,

$$\eta = \left(1 - \frac{C}{C_0}\right) \times 100 \quad (1)$$

Table 2 shows the smoke filtration efficiencies for all the cases studied, including those shown in Figure 5 (i.e., the cases without filter (the without-fiber case), with the PAN nanofiber filter without copper plating, and with copper plating for t = 10, 30, and 60 s). In Table 2, condition (a), the non-plated PAN nanofibers (t_{ep} = 0 s) reveals η = 22.9%; η increased to 44.0 and 68.6% in the 10 and 30 s plating cases, respectively, whereas it slightly decreased to 60.8% in the t_{ep} = 60 s plating case. Table 2,

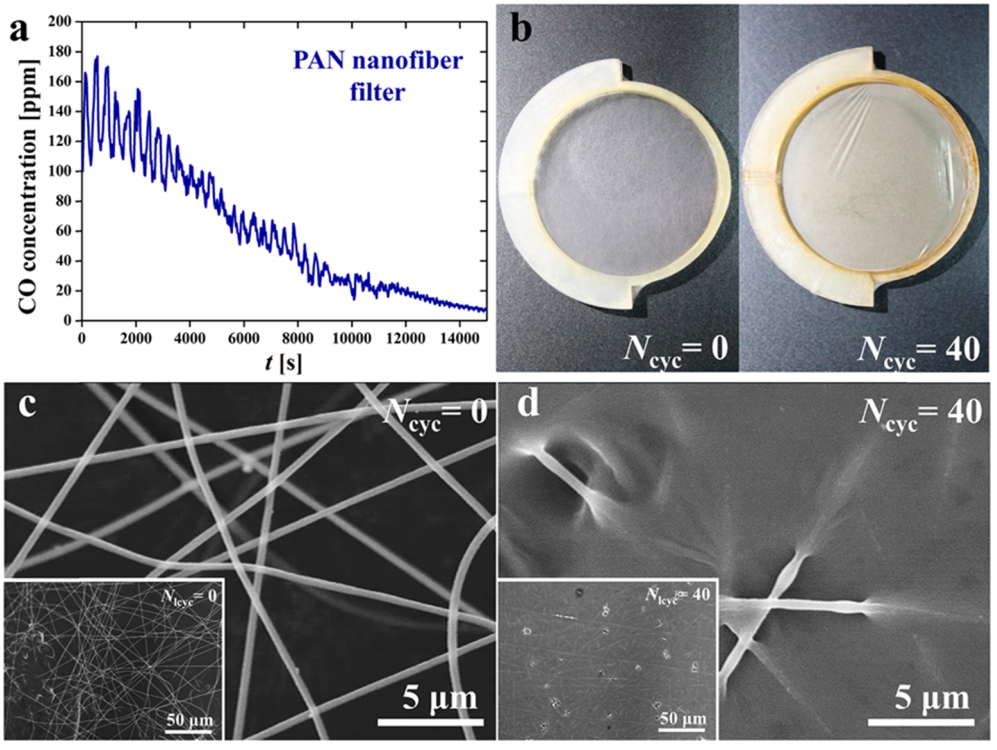

Figure 6. (a) Result for the CO concentration after the PAN nanofiber filter in the cycling test. (b) Photos of Cu microfiber filter before (N_{cyc} = 0) and after filtering (N_{cyc} = 40). SEM images of the PAN nanofiber filter at (c) N_{cyc} = 0 and (d) N_{cyc} = 40.

DOI: 10.1021/acsami.9b05686
ACS Appl. Mater. Interfaces XXXX, XXX, XXX−XXX

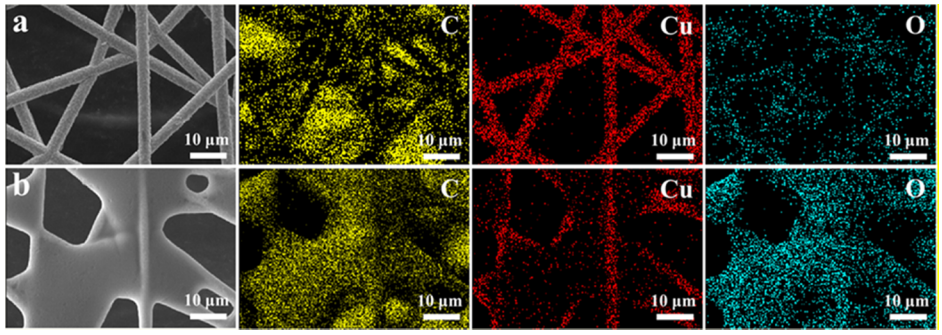

Figure 7. SEM images and the corresponding elemental mapping images of Cu microfibers (a) before and (b) after smoke filtration tests (N_{cyc} = 20).

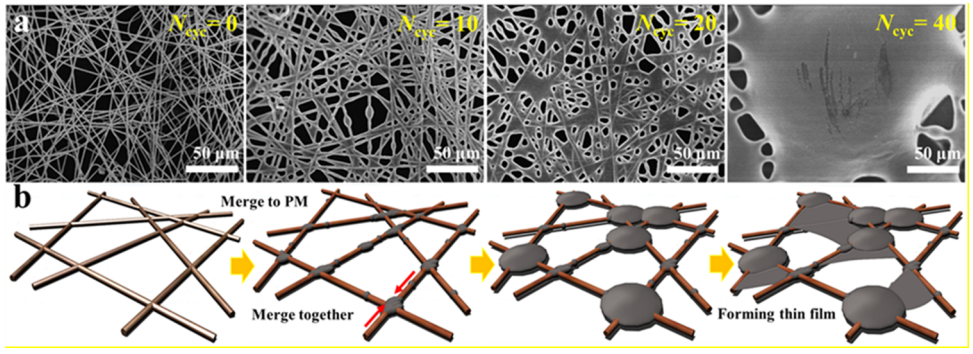

Figure 8. (a) SEM images of the Cu microfiber filter with increasing numbers of tests. (b) Schematic of the mechanism of PM deposition.

condition (b) shows the efficiencies based on the positions of the grounded PAN nanofiber mat. Compared to the bottom case (B in Table 2b), the values of η for the M and T locations (at the middle and near the top, respectively) decreased to approximately 36.3 and 35.4%, respectively. Table 2c lists the efficiencies with varying numbers of Cu microfiber filters. As expected, the efficiency η improved as the number of Cu microfiber filters increased, where the three-layer case corresponded to the highest value of η = 78.8% (Table 2, condition (c)).

3.3. Fouling of Cu Microfiber Filter. Figure 6 shows the results of the cycling test of the PAN nanofiber filter with 60 s of electrospinning, where Figure 6a presents the change in CO concentration during 40 cycles (N_{cyc} = 40). Note that N_{cyc} = 1 cycle (6 min) consisted of 3 min without and 3 min with applied voltage of 20 kV. Although similar trends in CO concentration are shown for the initial three cycles (N_{cyc} = 1−3), the subsequent concentration steadily decreased thereafter. The concentration without applied voltage decreased to less than 100 ppm at N_{cyc} = 12, and the CO concentration was less than the sensitivity of the device from N_{cyc} = 30. As shown in Figure 6b, the white PAN nanofiber filter (at N_{cyc} = 0) changed to brown following the cycling test (at N_{cyc} = 40) because of the captured PM on the PAN nanofiber filter. SEM images in Figure 6c,d clearly indicate that the PM was captured between the PAN nanofibers, thus blocking the pores of the nanofiber mat and resulting in a significant decrease in CO concentration.

Figure 7a,b shows the SEM and corresponding elemental mapping images of Cu microfibers before and after smoke filtration testing (N_{cyc} = 20), respectively. The SEM image in Figure 7b reveals that a film wrapped the Cu microfibers when the smoke filtration test was completed. It should be emphasized that in the case of inorganic soot-like PMs, the PMs formed a coating layer around the microfibers, and a thin film grew as a result.[19,54] The elemental mapping images shown in Figure 7b clearly indicate that the film-like deposit contained mainly C and O, which was attributed to the PM from the incense smoke captured by the electrically charged Cu microfibers during the test (cf. Figure 4a). The observed C on the Cu microfibers before the test was attributed to the presence of the background carbon tape applied to fix the fibers.

Figure 8a shows the change in the surface morphology of the Cu microfibers as the number of smoke filtration tests N_{cyc} increased from 0 to 40. The case of N_{cyc} = 0 in Figure 8a corresponds to the as-prepared untested Cu microfibers. At N_{cyc} = 10, PMs from the smoke appeared uniformly captured along the surfaces of the Cu microfibers, forming thin films while seemingly undergoing capillary instability that was expressed as a bead-like shape on two of the fibers. This suggests a liquid-like behavior of some part of the deposit; this could possibly be water vapor, which is one of the products of burning. As the number of tests increased, the PM coverage spanned multiple Cu microfibers at N_{cyc} = 20 and then finally covered nearly all Cu microfibers at N_{cyc} = 40 also in a liquid-like manner. The formation mechanism of PM films on the Cu microfibers is illustrated in Figure 8b. The schematic sequentially depicts the formation of film-like PM deposits at the beginning until its complete coverage of Cu microfibers. The figure shows that PMs began to make contact with each other along the surfaces of the Cu microfibers. Most PMs initially accumulated at junctions of the Cu microfibers, and newly captured PMs gradually agglomerated onto the existing PM clusters and Cu microfibers. With respect to PM coagulation, PMs increased in size and filled the void spaces between the fibers, resulting in film-like PM deposits.[54]

Dimethylformamide (DMF) soaking and sonication were performed to remove captured PMs from Cu microfiber filters, as demonstrated in Figure 9, as DMF is considered to dissolve

DOI: 10.1021/acsami.9b05686
ACS Appl. Mater. Interfaces XXXX, XXX, XXX−XXX

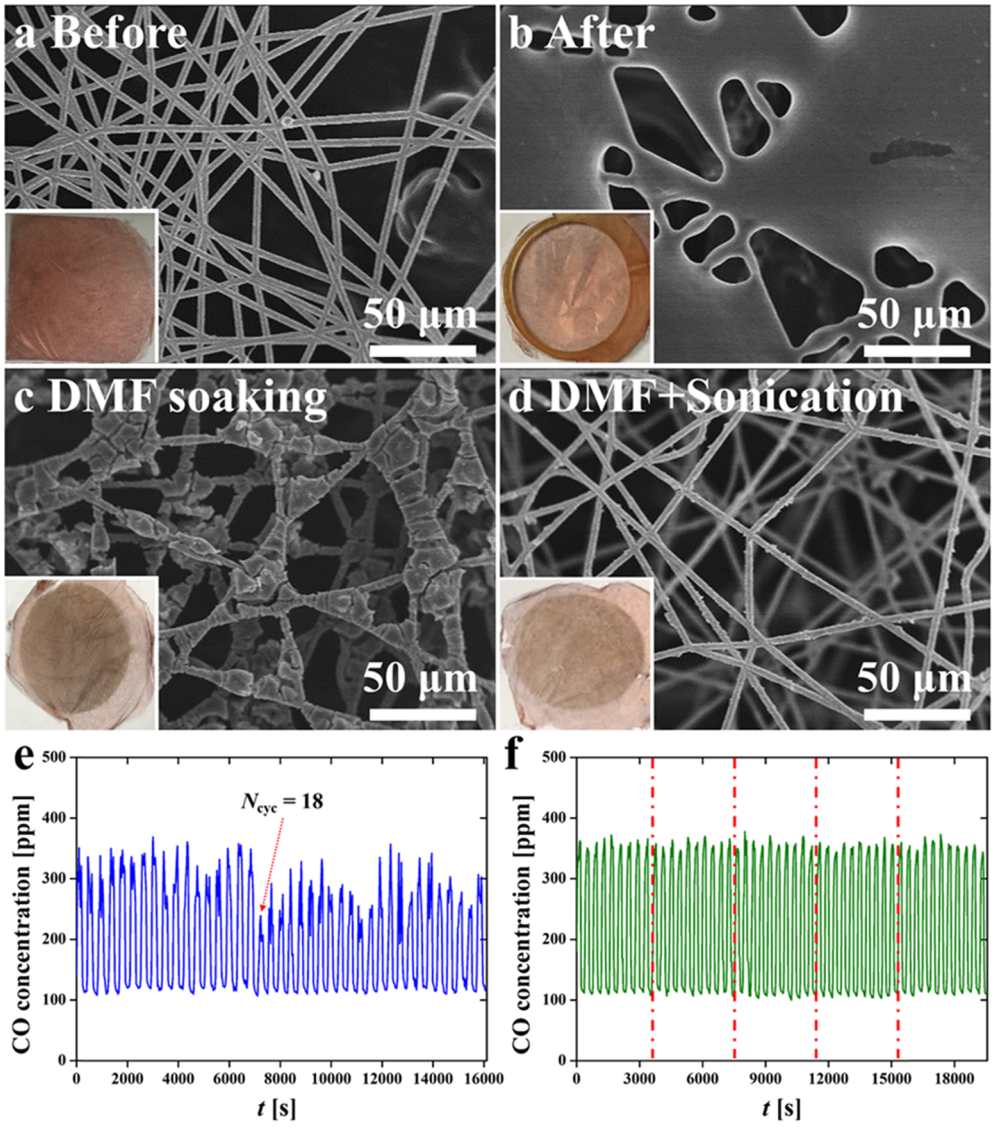

Figure 9. SEM images of Cu microfibers (a) before and (b) after smoke filtration tests, (c) after only DMF soaking, and (d) after sonication subsequent to DMF soaking. Recycle test (e) without DMF soaking and sonication and (f) with DMF soaking and sonication.

carbon effectively.[55] Figure 9a,b presents SEM images of Cu microfibers before and after smoke filtration tests, respectively; Figure 9c,b shows Cu microfibers after only DMF soaking and after sonication subsequent to DMF soaking, respectively. To remove the captured PMs from Cu microfibers, the tested Cu microfiber filter was soaked in DMF solution for 24 h and sonicated for 1 min, thus removing the film-like PM (although some PMs remained on the Cu microfibers). With sonication subsequent to DMF soaking, the PMs were completely removed, as revealed in Figure 9d, indicating the reusability of Cu microfiber filters. The insets in Figure 9a−d are photographs for each case.

Figure 9e,f shows the results of the cycling and recycling tests of Cu microfiber filters, respectively. The tests were conducted using one layer of Cu microfibers formed with t_{ep} = 30 s electroplating and installed near the bottom location of the setup. Figure 9e presents the results of the cycling test without DMF soaking and sonication. The CO concentration was measured for 180 s with the voltage applied and for 210 s without. This cycle was repeated 40 times. In the cycling test (Figure 9e), the maximum CO concentration was ∼300−350 ppm before the voltage was applied, and it decreased to <150 ppm after the voltage was applied.

As shown in Figure 9e, after N_{cyc} = 18, the CO concentration became unstable, which was attributed to an increase in the number of accumulated PMs on Cu microfibers as the cycle progressed. In other words, the smoke gradually ceased reaching the gas detector as the permeability of the filter decreased.

Figure 9f shows the recycling test with DMF soaking after the filtration test and the subsequent sonication. In this case, the Cu microfiber filter was cleaned by DMF soaking and sonication every N_{cyc} = 10 before repeating a new N_{cyc} = 10 process. The vertical red dotted lines in Figure 9f indicate the DMF soaking and sonication moments. Unlike the previous cycling test, the CO concentrations before and after the cleaning process remained nearly constant for N_{cyc} = 50 because PMs were completely removed from Cu microfibers by the cleaning process, yielding a filter with sustainable porosity.

To demonstrate the feasibility of the Cu microfiber filters for practical industrial applications, filtration tests with charcoal particles were performed as shown in Figure 10. The size of the charcoal particles ranged from tens of nanometers to a few

DOI: 10.1021/acsami.9b05686
ACS Appl. Mater. Interfaces XXXX, XXX, XXX−XXX

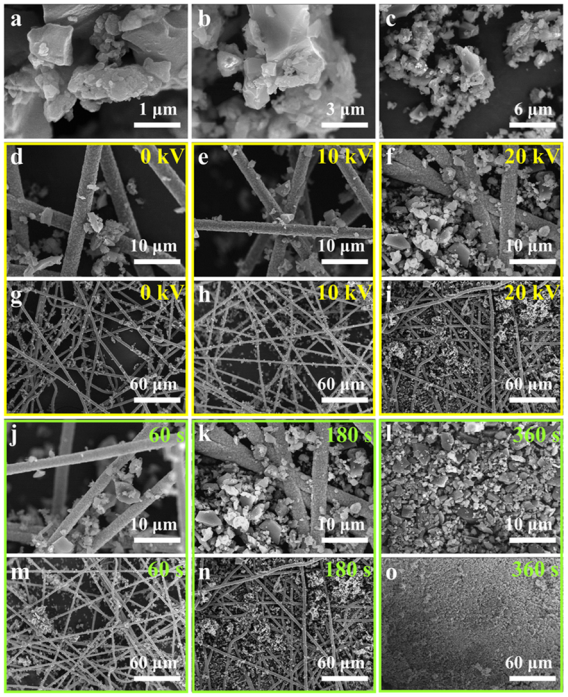

Figure 10. SEM images of (a–c) pulverized charcoal particles. SEM images of Cu microfiber filters after filtration tests of charcoal particles with (d–i) different voltages given in the panels and (j–o) different filtration times given in the panels.

micrometers, as shown in Figure 10a–c. Note that the filtration setup was the same as that used for the smoke filtration test (cf. Figures 2 and 4) except that charcoal particles on the bottom of the setup were driven upward by a fan. Charcoal particles were negatively charged by means of the triboelectric effect. Figure 10d–i shows SEM images of Cu microfiber filters after filtration tests when different voltages from 0 to 20 kV for a fixed filtration time of 180 s. Although the 0 and 10 kV cases slightly differed in terms of filtration efficiency, the 20 kV case clearly revealed the electrical enhancement of filtration. In addition, the number of captured charcoal particles clearly increased as the filtration time increased from 60 to 360 s at the fixed applied voltage of 20 kV, as observed in Figure 10j–o. The filtration mass was estimated under the operating conditions of 10 and 20 kV at the collection time of 180 s. The mass of the metallized fibers before usage was 6.5 mg. After the filtration experiment, the fiber masses with the collected PMs were 19, 25, and 80.9 mg when the charging voltages were 0, 10, and 20 kV, respectively. Thus, the electrification dramatically increased the collection efficiency as compared to the nonelectrification case. Furthermore, the charcoal PMs were not chemically bonded to the metal fibers and were thus easily removed from the fibers by simple air blowing. The snapshots in Figure 11 compare the fiber mass before and after filtration and after air blowing. These results show that approximately 90% of charcoal PMs were removed by air blowing.

4. CONCLUSION

In this study, fabrication of air filters consisting of metallized fibers was demonstrated. These fibers can be considerably charged by an applied voltage, and we showed that filters based on these fibers attracted charged particles from the incense smoke. The PM removal efficiency of the metallized fiber-based filters was assessed under different conditions. Multiple layers of

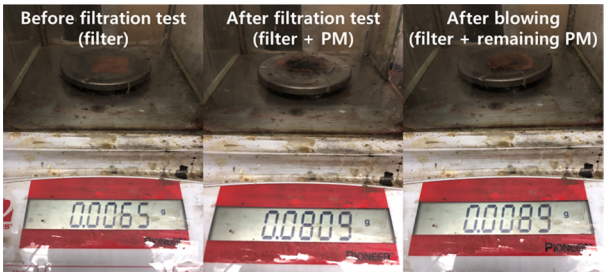

Figure 11. Snapshots comparing the fiber mass before and after filtration and after air blowing.

the fabricated air filter were placed at various locations inside a smoke-confining cylindrical pipe. The thickest metallized fiber, multiple layers, and the shortest distance between a Cu microfiber filter and grounded PAN nanofiber electrode yielded the highest removal rate. In all cases, we confirmed the excellent air filtration performance of the metallized fiber filters. A transparent air filter consisting of metallized fibers can be installed in portable air purification devices to achieve a high PM removal efficiency. In addition, we confirmed that the Cu microfiber filter could capture micrometer-scale charcoal particles, which means it holds a great promise for use as an electrified Cu microfiber filter in various industrial applications.

■ ASSOCIATED CONTENT

Supporting Information

The Supporting Information is available free of charge on the ACS Publications website at DOI: 10.1021/acsami.9b05686.

PM capturing of the Cu microfiber filter (MP4)

■ AUTHOR INFORMATION

Corresponding Authors

*E-mail: skyoon@korea.ac.kr (S.S.Y.).
*E-mail: ayarin@uic.edu (A.L.Y.).

ORCID

Sam S. Yoon: 0000-0002-9031-4198
Alexander L. Yarin: 0000-0001-8032-2525

Author Contributions

§M.W.K and S.A. contributed equally to this work.

Notes

The authors declare no competing financial interest.

■ ACKNOWLEDGMENTS

This research was supported by the Technology Development Program to Solve Climate Changes of the National Research Foundation (NRF) funded by the Ministry of Science, ICT & Future Planning (NRF-2016M1A2A2936760), NRF-2013R1A5A1073861, no. CRC-16-02-KICT, and NRF-2017R1A2B4005639.

■ REFERENCES

(1) Zhang, R.; Jing, J.; Tao, J.; Hsu, S.-C.; Wang, G.; Cao, J.; Lee, C. S. L.; Zhu, L.; Chen, Z.; Zhao, Y.; Shen, Z. Chemical Characterization and Source Apportionment of PM 2.5 in Beijing: Seasonal Perspective. *Atmos. Chem. Phys.* **2013**, *13*, 7053–7074.

(2) Watson, J. G. Visibility: Science and Regulation. *J. Air Waste Manage. Assoc.* **2002**, *52*, 628–713.

(3) Streets, D. G.; Wu, Y.; Chin, M. Two-Decadal Aerosol Trends as A Likely Explanation of The Global Dimming/Brightening Transition. *Geophys. Res. Lett.* **2006**, *33*, L15806.

DOI: 10.1021/acsami.9b05686
ACS Appl. Mater. Interfaces XXXX, XXX, XXX–XXX

(4) Andreae, M. O.; Rosenfeld, D. Aerosol−Cloud−Precipitation Interactions. Part 1. The Nature and Sources of Cloud-Active Aerosols. *Earth-Sci. Rev.* **2008**, *89*, 13−41.
(5) Mahowald, N. Aerosol Indirect Effect on Biogeochemical Cycles and Climate. *Science* **2011**, *334*, 794−796.
(6) Horton, D. E.; Skinner, C. B.; Singh, D.; Diffenbaugh, N. S. Occurrence and Persistence of Future Atmospheric Stagnation Events. *Nat. Clim. Change* **2014**, *4*, 698−703.
(7) Nel, A. Air Pollution-Related Illness: Effects of Particles. *Science* **2005**, *308*, 804−806.
(8) Ashmore, M. R.; Dimitroulopoulou, C. Personal Exposure of Children to Air Pollution. *Atmos. Environ.* **2009**, *43*, 128−141.
(9) Taneja, A.; Saini, R.; Masih, A. Indoor Air Quality of Houses Located in The Urban Environment of Agra, India. *Ann. N. Y. Acad. Sci.* **2008**, *1140*, 228−245.
(10) Miller, F. J. Dosimetry of Particles: Critical Factors Having Risk Assessment Implications. *Inhalation Toxicol.* **2000**, *12*, 389−395.
(11) Massey, D.; Kulshrestha, A.; Masih, J.; Taneja, A. Seasonal Trends of PM10, PM5. 0, PM2. 5 & PM1. 0 in Indoor and Outdoor Environments of Residential Homes Located in North-Central India. *Build. Sci.* **2012**, *47*, 223−231.
(12) Hinds, W. C. *Aerosol Technology: Properties, Behavior, and Measurement of Airborne Particles*; John Wiley & Sons: 2012.
(13) Beggs, C. B. The Airborne Transmission of Infection in Hospital Buildings: Fact or Fiction? *Indoor Built Environ.* **2003**, *12*, 9−18.
(14) Smith, G. J. D.; Vijaykrishna, D.; Bahl, J.; Lycett, S. J.; Worobey, M.; Pybus, O. G.; Ma, S. K.; Cheung, C. L.; Raghwani, J.; Bhatt, S.; Peiris, J. S. M.; Guan, Y.; Rambaut, A. Origins and Evolutionary Genomics of The 2009 Swine-Origin H1N1 Influenza A Epidemic. *Nature* **2009**, *459*, 1122−1125.
(15) Thakur, R.; Das, D.; Das, A. Electret Air Filters. *Sep. Purif. Rev.* **2013**, *42*, 87−129.
(16) Wang, C.-S. Electrostatic Forces in Fibrous Filters—A Review. *Powder Technol.* **2001**, *118*, 166−170.
(17) Barhate, R. S.; Ramakrishna, S. Nanofibrous Filtering Media: Filtration Problems and Solutions from Tiny Materials. *J. Membr. Sci.* **2007**, *296*, 1−8.
(18) Wang, N.; Si, Y.; Wang, N.; Sun, G.; El-Newehy, M.; Al-Deyab, S. S.; Ding, B. Multilevel Structured Polyacrylonitrile/Silica Nanofibrous Membranes for High-Performance Air Filtration. *Sep. Purif. Technol.* **2014**, *126*, 44−51.
(19) Gao, H.; Yang, Y.; Akampumuza, O.; Hou, J.; Zhang, H.; Qin, X. A Low Filtration Resistance Three-Dimensional Composite Membrane Fabricated via Free Surface Electrospinning for Effective PM2.5capture. *Environ. Sci.: Nano* **2017**, *4*, 864−875.
(20) Wang, C.; Wu, S.; Jian, M.; Xie, J.; Xu, L.; Yang, X.; Zheng, Q.; Zhang, Y. Silk Nanofibers as High Efficient and Lightweight Air Filter. *Nano Res.* **2016**, *9*, 2590−2597.
(21) Cai, R.-R.; Zhang, L.-Z.; Bao, A.-B. PM Collection Performance of Electret Filters Electrospun with Different Dielectric Materials-a Numerical Modeling and Experimental Study. *Build. Environ.* **2018**, *131*, 210−219.
(22) Wang, S.; Zhao, X.; Yin, X.; Yu, J.; Ding, B. Electret Polyvinylidene Fluoride Nanofibers Hybridized by Polytetrafluoroethylene Nanoparticles for High-Efficiency Air Filtration. *ACS Appl. Mater. Interfaces* **2016**, *8*, 23985−23994.
(23) Zhao, X.; Liu, Y. Evapotranspiration Partitioning and Response to Abnormally Low Water Levels in A Floodplain Wetland in China. *Adv. Meteorol.* **2016**, *2016*, 1.
(24) Zhao, X.; Li, Y.; Hua, T.; Jiang, P.; Yin, X.; Yu, J.; Ding, B. Cleanable Air Filter Transferring Moisture and Effectively Capturing PM2. 5. *Small* **2017**, *13*, 1603306.
(25) Sinha-Ray, S.; Sinha-Ray, S.; Yarin, A. L.; Pourdeyhimi, B. Application of Solution-Blown 20−50nm Nanofibers in Filtration of Nanoparticles: The Efficient Van Der Waals Collectors. *J. Membr. Sci.* **2015**, *485*, 132−150.
(26) Kolbasov, A.; Sinha-Ray, S.; Joijode, A.; Hassan, M. A.; Brown, D.; Maze, B.; Pourdeyhimi, B.; Yarin, A. L. Industrial-Scale Solution Blowing of Soy Protein Nanofibers. *Ind. Eng. Chem. Res.* **2015**, *55*, 323−333.
(27) Kolbasov, A.; Sinha-Ray, S.; Yarin, A. L.; Pourdeyhimi, B. Heavy Metal Adsorption on Solution-Blown Biopolymer nanofiber membranes. *J. Membr. Sci.* **2017**, *530*, 250−263.
(28) Kim, Y.-h.; Yiacoumi, S.; Tsouris, C. Surface Charge Accumulation of Particles Containing Radionuclides in Open Air. *J. Environ. Radioact.* **2015**, *143*, 91−99.
(29) Goldade, V.; Rychkov, A.; Rychkov, D. Electret Properties of Polymer Films and Fiber Materials Modified by Phosphorus Trichloride. In *2010 10th IEEE International Conference on Solid Dielectrics: (ICSD)*; IEEE: Piscataway, NJ, 2010; pp 1−3.
(30) Jaworek, A.; Krupa, A.; Czech, T. Modern Electrostatic Devices and Methods for Exhaust Gas Cleaning: A Brief Review. *J. Electrost.* **2007**, *65*, 133−155.
(31) Nifuku, M.; Zhou, Y.; Kisiel, A.; Kobayashi, T.; Katoh, H. Charging Characteristics for Electret Filter Materials. *J. Electrost.* **2001**, *51-52*, 200−205.
(32) Tsai, P. P.; Schreuder-Gibson, H.; Gibson, P. Different Electrostatic Methods for Making Electret Filters. *J. Electrost.* **2002**, *54*, 333−341.
(33) Ji, J. H.; Bae, G. N.; Kang, S. H.; Hwang, J. Effect of Particle Loading on The Collection Performance of An Electret Cabin Air Filter for Submicron Aerosols. *J. Aerosol Sci.* **2003**, *34*, 1493−1504.
(34) Frederick, E. R. Fibers, Electrostatics, and Filtration: A Review of New Technology. *J. Air Pollut. Control Assoc.* **1980**, *30*, 426−431.
(35) Schreuder-Gibson, H. L.; Gibson, P.; Tsai, P. Cooperative Charging Effects of Fibers From Electrospinning of Electrically Dissimilar Polymers. *Int. Nonwovens J.* **2004**, *13*, 39−45.
(36) Cho, B. M.; Nam, Y. S.; Cheon, J. Y.; Park, W. H. Residual Charge and Filtration Efficiency of Polycarbonate Fibrous Membranes Prepared by Electrospinning. *J. Appl. Polym. Sci.* **2015**, *132*, 41340.
(37) Li, X.; Wang, N.; Fan, G.; Yu, J.; Gao, J.; Sun, G.; Ding, B. Electreted Polyetherimide−Silica Fibrous Membranes for Enhanced Filtration of Fine Particles. *J. Colloid Interface Sci.* **2015**, *439*, 12−20.
(38) Li, Q.; Xu, Y.; Wei, H.; Wang, X. An Electrospun Polycarbonate Nanofibrous Membrane for High Efficiency Particulate Matter Filtration. *RSC Adv.* **2016**, *6*, 65275−65281.
(39) An, S.; Kim, Y. I.; Jo, H. S.; Kim, M.-W.; Swihart, M. T.; Yarin, A. L.; Yoon, S. S. Oxidation-Resistant Metallized Nanofibers as transparent Conducting Films and Heaters. *Acta Mater.* **2018**, *143*, 174−180.
(40) Jo, H. S.; An, S.; Lee, J.-G.; Park, H. G.; Al-Deyab, S. S.; Yarin, A. L.; Yoon, S. S. Highly Flexible, Stretchable, Patternable, Transparent Copper Fiber Heater on A Complex 3D Surface. *NPG Asia Mater.* **2017**, *9*, No. e347.
(41) Joshi, B.; Samuel, E.; Kim, Y. I.; Kim, M.-W.; Jo, H.-S.; Swihart, M. T.; Yoon, W. Y.; Yoon, S. S. Hierarchically Designed ZIF-8-Derived Ni@ ZnO/Carbon Nanofiber Freestanding Composite for Stable Li Storage. *Chem. Eng. J.* **2018**, *351*, 127−134.
(42) An, S.; Jo, H. S.; Al-Deyab, S. S.; Yarin, A. L.; Yoon, S. S. Nano-Textured Copper Oxide Nanofibers for Efficient Air Cooling. *J. Appl. Phys.* **2016**, *119*, No. 065306.
(43) An, S.; Jo, H. S.; Kim, D.-Y.; Lee, H. J.; Ju, B.-K.; Al-Deyab, S. S.; Ahn, J.-H.; Qin, Y.; Swihart, M. T.; Yarin, A. L.; Yoon, S. S. Self-junctioned copper nanofiber transparent flexible conducting film via electrospinning and electroplating. *Adv. Mater.* **2016**, *28*, 7149−7154.
(44) Lee, M. W.; Jo, H. S.; Yoon, S. S.; Yarin, A. L. Thermally Driven Self-Healing Using Copper Nanofiber Heater. *Appl. Phys. Lett.* **2017**, *111*, No. 011902.
(45) An, S.; Jo, H. S.; Kim, Y. I.; Song, K. Y.; Kim, M.-W.; Lee, K. B.; Yarin, A. L.; Yoon, S. S. Bio-Inspired, Colorful, Flexible, Defrostable Light-Scattering Hybrid Films for The Effective Distribution of LED Light. *Nanoscale* **2017**, *9*, 9139−9147.
(46) An, S.; Kim, Y. I.; Sinha-Ray, S.; Kim, M.-W.; Jo, H. S.; Swihart, M. T.; Yarin, A. L.; Yoon, S. S. Facile Processes for Producing Robust, Transparent, Conductive Platinum Nanofiber mats. *Nanoscale* **2017**, *9*, 6076−6084.

DOI: 10.1021/acsami.9b05686
ACS Appl. Mater. Interfaces XXXX, XXX, XXX−XXX

(47) Kim, M.-W.; An, S.; Kim, K.; Kim, T.-G.; Jo, H. S.; Park, D.-H.; Yoon, S. S.; Yarin, A. L. Packing of Metalized Polymer Nanofibers for Aneurysm Embolization. *Nanoscale* **2018**, *10*, 6589−6601.
(48) Seinfeld, J. H.; Pandis, S. N. *Atmospheric Chemistry and Physics: From Air Pollution to Climate Change*; John Wiley & Sons: New York: 2016.
(49) Scuseria, G. E.; Miller, M. D.; Jensen, F.; Geertsen, J. The Dipole Moment of Carbon Monoxide. *J. Chem. Phys.* **1991**, *94*, 6660−6663.
(50) Lawton, J.; Weinberg, F. *Electrical Aspects of Combustion*; Clarendon Press: Oxford, 1969.
(51) Choi, K. J.; Delcorio, B. Generation of Controllable Monodispersed Sprays Using Impulse Jet and Charging Techniques. *Rev. Sci. Instrum.* **1990**, *61*, 1689−1693.
(52) Mainelis, G.; Willeke, K.; Baron, P.; Grinshpun, S. A.; Reponen, T. Induction Charging and Electrostatic Classification of Micrometer-Size Particles for Investigating The Electrobiological Properties of Airborne Microorganisms. *Aerosol Sci. Technol.* **2010**, *36*, 479−491.
(53) Sambudi, N. S.; Choi, H.-J.; Lee, M.-H.; Cho, K. Capture of Ultrafine Particles Using A Film-Type Electret Filter with A Unipolar Charger. *Aerosol Air Qual. Res.* **2017**, *17*, 626−635.
(54) Liu, C.; Hsu, P.-C.; Lee, H.-W.; Ye, M.; Zheng, G.; Liu, N.; Li, W.; Cui, Y. Transparent Air Filter For High-Efficiency PM 2.5 Capture. *Nat. Commun.* **2015**, *6*, 6205.
(55) Bahr, J. L.; Mickelson, E. T.; Bronikowski, M. J.; Smalley, R. E.; Tour, J. M. Dissolution of Small Diameter Single-Wall Carbon Nanotubes in Organic Solvents? *Chem. Commun.* **2001**, 193−194.

DOI: 10.1021/acsami.9b05686
ACS Appl. Mater. Interfaces XXXX, XXX, XXX−XXX